(12)
NW

WIND TUNNEL RESULTS OF A 10-PERCENT SCALE POWERED SCAT VTOL AIRCRAFT

by

David G. Lee and David W. Lacey

AVIATION AND SURFACE EFFECTS DEPARTMENT

ASED 371

March 1977

DAVID W. TAYLOR NAVAL SHIP RESEARCH AND DEVELOPMENT CENTER

BETHESDA MARYLAND 20084

UNCLASSIFIED

SECURITY CLASSIFICATION OF THIS PAGE (When Data Entered)

REPORT DOCUMENTATION PAGE

READ INSTRUCTIONS BEFORE COMPLETING FORM

1 REPORT NUMBER: DTNSRDC/ASED-371

2 GOVT ACCESSION NO.:

3 RECIPIENT'S CATALOG NUMBER:

4 TITLE (and Subtitle): Wind Tunnel Results of a 10-percent Scale Powered SCAT VTOL Aircraft.

5 TYPE OF REPORT & PERIOD COVERED: Interim Report, Jul [redacted] — Oct 76

6 PERFORMING ORG. REPORT NUMBER:

7 AUTHOR(s): David G. Lee and David W. Lacey

8 CONTRACT OR GRANT NUMBER(s):

9 PERFORMING ORGANIZATION NAME AND ADDRESS:
Aviation and Surface Effects Department
David W. Taylor Naval Ship R&D Center
Bethesda, Maryland 20084

10 PROGRAM ELEMENT, PROJECT, TASK AREA & WORK UNIT NUMBERS:
Program Element 61152N
Task Area ZR0230301
Work Unit 1660-870

11 CONTROLLING OFFICE NAME AND ADDRESS:
Naval Air Development Center
Warminster, Pennsylvania 18974

12 REPORT DATE: March 1977

13 NUMBER OF PAGES: 23

14 MONITORING AGENCY NAME & ADDRESS (if different from Controlling Office):

15 SECURITY CLASS. (of this report): Unclassified

15a DECLASSIFICATION DOWNGRADING SCHEDULE:

16 DISTRIBUTION STATEMENT (of this Report)

Approved for public release: Distribution Unlimited

17 DISTRIBUTION STATEMENT (of the abstract entered in Block 20, if different from Report)

White Section ☑
Buff Section ☐
[illegible]NOUNCED ☐
[illegible]ICATION

18 SUPPLEMENTARY NOTES

[illegible]CTION/AVAILABILITY CODES
[illegible] AVAIL. and/or SPECIAL
A

19 KEY WORDS (Continue on reverse side if necessary and identify by block number)

Aerodynamics	Stability
Radomes	VSTOL Aircraft
SCAT	OTH Targeting

20 ABSTRACT (Continue on reverse side if necessary and identify by block number)

The low-speed aerodynamic characteristics of a 10-percent scale powered SCAT (Surveillance, Communications, ASMD Warning, and Targeting) configuration were investigated in the 8- by 10-foot subsonic north wind tunnel at the David W. Taylor Naval Ship Research and Development Center. Force and moment data were obtained for both powered and unpowered VTOL, fixed-wing aircraft. Analysis of the data indicate that the configuration is statically stable in both pitch and yaw and that control is adequate for both axes. The addition

(continued on reverse side)

DD FORM 1 JAN 73 1473 EDITION OF 1 NOV 65 IS OBSOLETE
S/N 0102-014-6601

UNCLASSIFIED

SECURITY CLASSIFICATION OF THIS PAGE (When Data Entered)

(Block 20 continued)

of a large aft-mounted radome did not significantly change longitudinal characteristics, but did increase lateral-directional stability. Two wings of different airfoil sections were evaluated: a NACA design and a Liebeck design. The Liebeck wing section increased lift over that generated by the NACA baseline wing section.

TABLE OF CONTENTS

LIST OF FIGURES

NOTATION

The results in this report are reduced to standard aerodynamic force and moment coefficients and are presented in both stability and wind axis systems. All moments are referenced to the quarter root chord in the X-plane and the propeller thrust axis in the Z-plane. Angles of attack and sideslip are relative to the fuselage.

b Wing span, 3.867 ft

c Mean aerodynamic chord, 0.33 ft

d Propeller diameter, 0.6 ft

n Propeller rotational speed

q Dynamic pressure

s Wing area, 1.25 ft^2

T Propeller thrust

V Tunnel velocity

ρ density

$$C_L = \frac{\text{Lift}}{qs}$$

$$C_D = \frac{\text{Drag}}{qs}$$

$$D_m = \frac{\text{Pitching Moment}}{qsc}$$

$$C_{ROLL} = \frac{\text{Rolling Moment}}{qsb}$$

$$C_{YAW} = \frac{\text{Yawing Moment}}{qsb}$$

$$C_y = \frac{\text{Side Force}}{qs}$$

$$C_T = \frac{T}{\rho n^2 d^4}$$

$$J = \frac{V}{nd}$$

ABSTRACT

The low-speed aerodynamic characteristics of a 10-percent scale powered SCAT (Surveillance, Communications, ASMD Warning, and Targeting) configuration were investigated in the 8- by 10-foot subsonic north wind tunnel at the David W. Taylor Naval Ship Research and Development Center. Force and moment data were obtained for both powered and unpowered VTOL, fixed-wing aircraft. Analysis of the data indicate that the configuration is statically stable in both pitch and yaw and that control is adequate for both axes. The addition of a large aft-mounted radome did not significantly change longitudinal characteristics, but did increase lateral-directional stability. Two wings of different airfoil sections were evaluated: a NACA design and a Liebeck design. The Liebeck wing section increased lift over that generated by the NACA base-line wing section.

ADMINISTRATIVE INFORMATION

This work was the result of a joint program by the David W. Taylor Naval Ship Research and Development Center (DTNSRDC) Bethesda, Maryland, and the Naval Air Development Center (NADC), Warminster, Pennsylvania. NADC assumed responsibility for the conceptual design phase of the aircraft while the exploratory wind tunnel program was managed by DTNSRDC. Wind tunnel model design and construction were accomplished by DTNSRDC and funded under Independent Research. Funding for the exploratory wind tunnel program was provided by NADC.

INTRODUCTION

NADC has been involved in a study effort which addresses the problem of providing real-time surveillance, over-the-horizon (OTH) targeting and similar functions for ship groups not in company with an aircraft carrier. A small, manned, fixed-wing VTOL aircraft was conceived by NADC to fulfill this mission. SCAT employs two lift jet engines for vertical takeoff and landing from destroyer and frigate-class ships but transitions to a turboprop engine for conventional flight.

DTNSRDC was requested by NADC to perform an experimental wind tunnel evaluation of the SCAT vehicle concept including the design and construction of a 10-percent scale model. The objective of the wind tunnel program was to obtain the necessary data base required to determine the aerodynamic characteristics of the SCAT configuration; this report presents that data base.

APPARATUS

The 8- x 10-foot subsonic north wind tunnel at DTNSRDC is of the single return closed-circuit type that is capable of continuous operation at atmospheric pressure. The rectangularly shaped test section can achieve dynamic pressures up to 80 lb/sq ft. For this series of investigations, the SCAT model was mounted in the test section using Strut System 6. This strut system is located beneath the tunnel floor and supports the model via a vertical strut tip which, in turn, transfers the aerodynamic loads to an external Toledo mechanical balance system. The Toledo balance system records six component force and moment data on magnetic tape using a Beckman 210 High Speed Data Acquisition System. The majority of these data were recorded at a dynamic pressure of 10 lb/sq ft with some limited data points at 60 lb/sq ft. Standard blockage, buoyancy, and wall corrections were applied to the reduced data according to the methods outlined in Reference 1.

MODEL

The 10-percent scale SCAT wind tunnel model was constructed entirely of aluminum with removable wing and tail surfaces. Horizontal and vertical control surfaces are adjustable over a range of deflection angles. Two wings with identical planforms and physical dimensions were constructed; the only difference was the airfoil section. The baseline airfoil section was an NACA 64_3-618 while the other employed a high lift Liebeck section (LA 5054).[1] Two typical radome shapes were constructed of wood for mounting under the fuselage: one a pancake-saucer shape and the other a flattened egg shape. A four-bladed wooden propeller with a 6.2-inch diameter was powered by a 10 horsepower, water cooled, variable frequency electric motor mounted inside the SCAT fuselage. This propeller-motor combination was used to simulate the turboprop power plant on the SCAT vehicle. The lift jets were not simulated during this investigation. Figure 1 presents

[1] Dr. Liebeck at Douglas Aircraft Company, under the sponsorship of the Air Force Flight Dynamics Laboratory, has developed a series of superlift airfoils for high lift applications.

the major dimensions of the SCAT model.

The location of the radome and propeller dictated mounting the SCAT wind tunnel model with a vertical strut system and testing it in the inverted position. This was also considered to create minimum interference on the model. An extensive series of runs were therefore conducted for each SCAT model configuration to evaluate the tare and interference of the model support system. The procedure followed was similar to the standard method outlined in Reference 1. The model was mounted in the wind tunnel in each of three different positions: (1) erect, (2) inverted, and (3) erect with an image support system. Force and moment data were recorded for each position. The tare and interference of the model support is equal to the model in the erect position with an image support minus the data with the model in the erect position. This correction was then subtracted from the data obtained for the model tested in the inverted position. These data are then theoretically interference free force and moment data. Data for each of the three test positions is presented in tabulated form in this report; the run schedule and tabulated data are contained in Appendixes A and B. Figure 2 shows photographs of the model mounted in the inverted position and the model erect with the dummy-image support mounted in the wind tunnel.

The power-on phase of this program was conducted at constant thrust conditions. Full-scale thrust coefficient at cruise power conditions was simulated during wind tunnel tests. The SCAT model motor-propeller combination was calibrated before the wind tunnel test program to determine thrust characteristics. The drag of the complete SCAT configuration, less radome, was measured in the wind tunnel at various dynamic pressures with the propeller both on and off. The difference in drag levels then represents the installed thrust. A calibration curve for power was then produced for various motor rpm's. The wind tunnel test program was conducted at the model motor-propeller rpm combination which duplicates the same full-scale thrust coefficient.

Transition grit (#80 carborundum particles) was used on the wings and fuselage nose of the model throughout the test program. The location and size of the grit were determined by the procedure outlined in

Reference 2. A 1/8-inch-wide band of grit was placed on the fuselage 1.5 inches back from the nose. For the NACA airfoil, the transition strip was placed 1.2 inches back from the leading edge on both the upper and lower surfaces. The Liebeck wing had a transition strip of the same dimensions but only on the upper surface. When attached to the fuselage, the radomes also had transition grit of similar dimensions and were 1.4 inches back from the leading edge surface.

TEST PROGRAM

The majority of the data for the experimental wind tunnel program were recorded at a dynamic pressure of 10 lb/sq ft with limited data points at 60 lb/sq ft. These correspond to Reynolds numbers of approximately 190,000 and 470,000, respectively, for a wing chord of 0.33 ft.

The angle-of-attack range covered in this investigation varied from -6 degrees to +16 degrees. Data for this angle of attack range were recorded at sideslip angles of 0, 5, and 10 degrees. Elevator control surface deflection angles investigated were +10, 0, -5, -10 and -15 degrees. Elevator trailing edge down is considered positive for this program. Rudder surface deflections used in this program were 0, -5, and -10 degrees with the surfaces always deflected in pairs. Positive deflection for the rudders was trailing edge to the left.

Aircraft component buildup consisting of fuselage, wing, tail sections, and radome assembly was also investigated in this program.

ANALYSIS

BASIC CONFIGURATION DATA

Figure 3 presents buildup data for the basic unpowered configuration without radome. The data (Figures 3 through 10) have been corrected for the effect of the mounting support system unless otherwise noted.

Mounting support system corrections were made using the following equations:

$$C_{L_{\text{erect \& image}_{\alpha_n, \beta_n}}} - C_{L_{\text{erect}_{\alpha_n, \beta_n}}} = \Delta C_{L_{\text{strut}_{\alpha_n, \beta_n}}}$$

$$C_{L_{corrected_{\alpha_n, \beta_n}}} = C_{L_{inverted_{\alpha_n, \beta_n}}} - \Delta C_{L_{strut_{\alpha_n, \beta_n}}}$$

This was done for each of the coefficients (C_L, C_D, C_M, C_N, C_Y, and C_ℓ) at constant angle of attack and/or side slip angle.

An examination of the lift data indicates that the horizontal tail is down-loaded throughout the angle-of-attack range presented. Comparison of the body-wing and body-wing-tail configurations indicated that the tail lift contribution is relatively additive, thus indicating little downwash from the wing. Similarly, the pitching moment data show additive trends; however, there is a small constant negative downwash angle. The pitching moment data indicate that the vehicle is stable throughout the angle-of-attack range.

The drag data indicate large interference between body and tail. The incremental drag due to the tail was on the order of 120 counts (0.0120), which is approximately twice the analytically estimated drag of 65 counts (0.0065) for the horizontal-vertical tail contribution.

Wing installation to the body similarly caused large unexpected drag increments; these increments were on the order of 250 counts (0.0250). The drag of the complete configuration is only slightly greater than the drag of the wing-body alone, indicating a masking effect on the tail due to the presence of the wing. This masking effect may, in part, be due to the vortices being shed from the wing-body junction cancelling those vortices from the body-tail juncture.

EFFECT OF RADOME

Figure 4 presents the effect of adding the two radome shapes investigated. Both radome shapes caused a slight loss in lift, nose-up pitching moments, and increased drag. The base-line shape R_1 exhibited the largest increases in both pitching moment and drag and the smallest reduction in lift. Pitching moment stability was slightly increased by installation of the radomes.

EFFECT OF THRUST

The effect of thrust on lift, drag, and pitching moment is shown in Figure 5. The configuration depicted includes the R_1 radome. The data presented are for thrust coefficients, C_T of 0.152, 0.184, and 0.210. As indicated in Figure 5, thrust increased lift and decreased drag at all three thrust coefficients.

The trends for pitching moment are not as easily discernable. Thrust increased the pitching moment stability of the vehicle at low angles of attack; however, at angles greater than 4 degrees, pitching moment stability was reduced.

Reducing or increasing the thrust around the design thrust coefficient of 0.184 caused a nose-up pitching moment increment. A potential control problem with change of thrust is therefore indicated since nose down control would need to be applied with any thrust change rather than having the desired characteristic of moving the controls proportionally with the thrust change.

EFFECT OF REYNOLDS NUMBER

As stated in the apparatus section, the majority of the wind tunnel program was run at a dynamic pressure of 10 lb/sq ft; however, certain configurations were evaluated at a dynamic pressure of 60 lb/sq ft. A comparison of the basic wing-body-tail configuration at these two dynamic pressures is presented in Figure 6. The data are uncorrected for sting interference. Examination of the lift data indicates a slight zero lift angle-of-attack increase for the 60 lb/sq ft case as well as a slight increase in maximum lift coefficient. Drag was reduced by approximately 40 counts (0.0040) when the dynamic pressure was increased.

The pitching moment data indicate the largest shifts between the two cases. The higher q case has a linear pitching moment change with angle of attack, whereas the lower q case shows distinct steps. These steps occur throughout the range of configurations tested but are most noticeable when the horizontal tail is installed. Examination of the inverted versus erect mounted cases indicate that these steps may, in part, be due to vortices being shed from the mounting systems, thus

changing the flow on the aft position of the body. Flow changes on the body would not be seen in the lift but could conceivably change the center of pressure location hence resulting in significant moment changes due to the long moment arms involved.

LATERAL-DIRECTIONAL CHARACTERISTICS

Unpowered lateral-directional data for the basic configuration with and without the radome are shown in Figure 7. The data have been corrected for the presence of the strut. As shown the vehicle is stable with respect to both yawing and rolling moment, C_{n_β} and C_{ℓ_β}, respectively. The vehicle exhibits excellent directional stability throughout the angle-of-attack range presented having nearly constant C_{n_β}. The rolling moment stability C_{ℓ_β} decreases slightly with increasing angle of attack; however, it is still adequate. The addition of the radome increased the level of stability in roll while C_{n_β} stayed relatively constant.

The effect of power on the lateral-directional characteristics is shown in Figure 8. In general, power made no change in C_{n_β}; however, C_{ℓ_β} was increased when power was added.

LONGITUDINAL CONTROL EFFECTIVENESS

Longitudinal control effectiveness is shown in Figure 9 for the unpowered complete configuration. Presented are plots of C_M versus δ_e and C_L versus δ_e for angles of attack from 0 to 16 degrees. As shown C_{M_δ} is reasonably linear over the angle-of-attack range. The loss of lift due to control deflection amounts to 0.15 for a 20-degree deflection at 0 degrees angle of attack. Longitudinal control effectiveness was not affected by power; therefore, the data are not presented.

Rudder control effectiveness is presented in Figure 10. The configuration presented is powered and includes the R_1 radome. The variation of yawing moment with angle of attack for rudder deflections of 0, 5, and 10 degrees shows that the rudder is effective at all angles of attack and that C_{n_δ} is relatively constant. Examination of the

yawing moment data presented in Figure 8 indicates that the 10-degree deflection is capable of trimming the aircraft angle to -7.5 degrees. Rudder roll power varies somewhat with angle of attack and, in fact, a reversal in roll direction occurs at angles below 4 degrees for a 10-degree rudder deflection. Side force due to rudder deflection is relatively constant indicating little, if any, flow separation on the rudder.

COMPARISON OF LIEBECK WING WITH NACA WING

As stated earlier, two wings identical in planform but having different airfoil sections were evaluated. These were the basic wing having a NACA 64_3-618 section and a high lift Liebeck section (LA 5054). A comparison of these two wings is shown in Figure 11. Data are presented at dynamic pressures of 10 and 60 lb/sq ft and are not corrected for the mounting system.

The Liebeck section exhibited larger zero lift angle of attack, slightly higher lift curve slope C_{L_α}, and greater maximum lift coefficient. The Liebeck wing, however, exhibited slightly higher drag as well as a more positive pitching moment than the NACA wing.

As previously mentioned, the NACA section was relatively insensitive to Reynolds number; however, the Liebeck section was highly sensitive, as can be seen in both the plots of lift and drag. The section was designed for a Reynolds number of 500,000 which corresponds approximately to a dynamic pressure of 60 lb/sq ft. At the lower q the Reynolds number corresponds to 188,000 and the upper surface separated. At an angle of attack of between 10 and 12 degrees reattachment occurred.

A measure of the loiter capability of a propeller equipped aircraft is the maximum value of $C_L^{3/2}/C_D$. A comparison of this parameter for the baseline NACA airfoil and the Liebeck wing is shown in Figure 12. The data have been corrected for the effect of the strut. As shown in the figure, the Liebeck section exhibits a higher value of $C_L^{3/2}/C_D$ than the corresponding NACA section. The differences in maximum value corresponding to approximately 8-percent gain for the Liebeck section.

The maximum value for the Liebeck wing occurs at approximately 2 degrees before stall, whereas the maximum value for the NACA wing occurs at stall angle of attack. Since flight near stall angle of attack is difficult, the vehicle would need to be flown at a lower angle of attack, and the actual gains in performance for the Liebeck section increase. For example, if both sections were flown at 2 degrees below stall, the Liebeck section would have approximately an 18-percent gain in loiter capability over the NACA section.

CONCLUSIONS

The brief analysis of data from the wind tunnel evaluation indicates that:

1. The SCAT configuration is statically stable in both longitudinal and lateral modes.
2. Control is adequate in both pitch and yaw.
3. The large radome did not significantly change the longitudinal characteristics but increased the lateral-directional stability.
4. Thrust increased pitch stability at low angles of attack but reduced stability at angles greater than 4 degrees; dihedral effect C_{ℓ_β} increased with thrust, whereas directional stability C_{n_β} remained unchanged.
5. Increase in Reynolds number increased lift and decreased drag slightly.
6. Large interference drag increments occurred between body-tail and body-wing.
7. The Liebeck section increased lift and decreased drag at high angles of attack when compared to the NACA base-line wing section.
8. The Liebeck section wing provides significant increase in loiter performance.

REFERENCES

1. Pope, A. and J. J. Harper, "Low-Speed Wind Tunnel Testing," John Wiley and Sons, Inc., New York (1966).

2. Braslow, A. L. and E. C. Knox, "Simplified Method for Determination of Critical Height of Distributed Roughness Particles for Boundary-Layer Transition at Mach Numbers from 0 to 5," National Advisory Committee for Aeronautics Tech Note 4363 (Sep 1958).

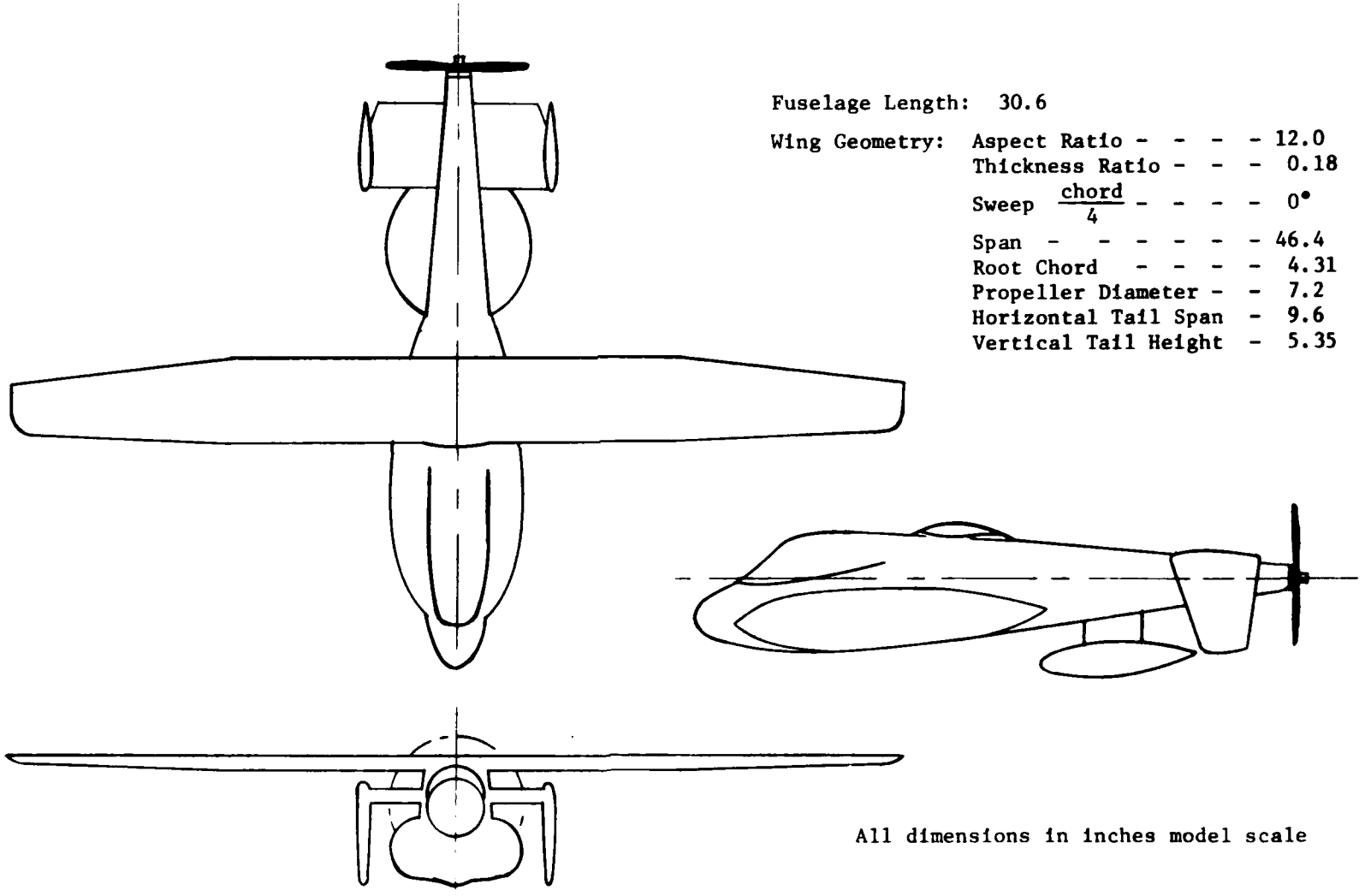

Fuselage Length: 30.6

Wing Geometry:

Aspect Ratio	12.0
Thickness Ratio	0.18
Sweep $\frac{\text{chord}}{4}$	0°
Span	46.4
Root Chord	4.31
Propeller Diameter	7.2
Horizontal Tail Span	9.6
Vertical Tail Height	5.35

All dimensions in inches model scale

Figure 1 - Major SCAT Model Dimensions

Figure 2 - SCAT Tunnel Installation

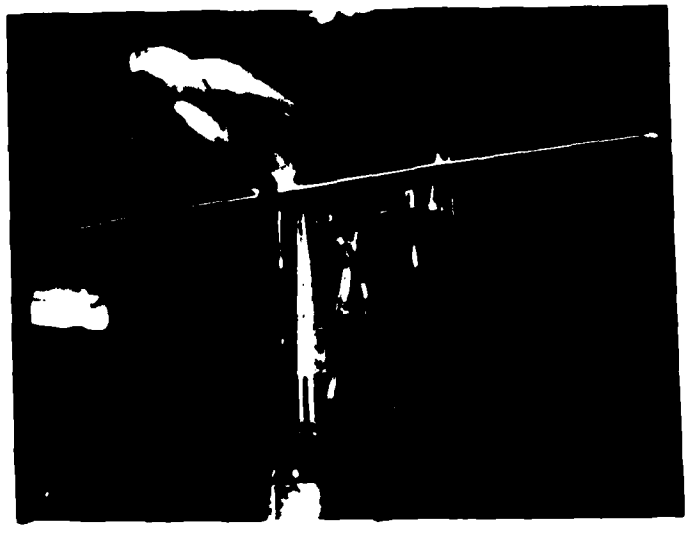

Figure 2a-Model Inverted with Balance Support

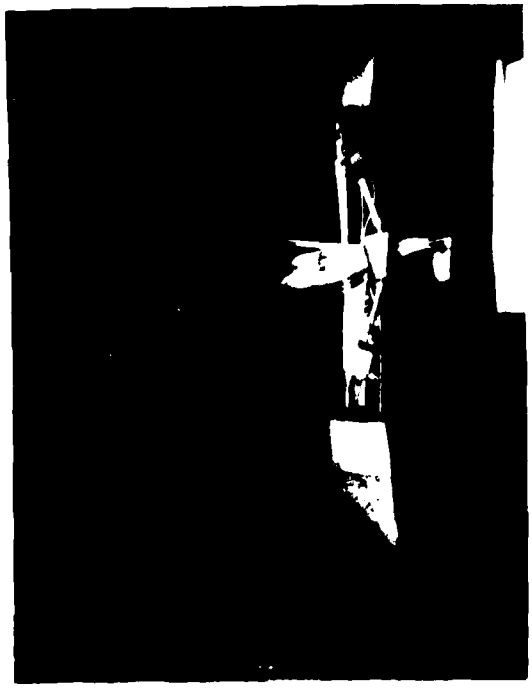

Figure 2b-Model Erect with Dummy-Image Support

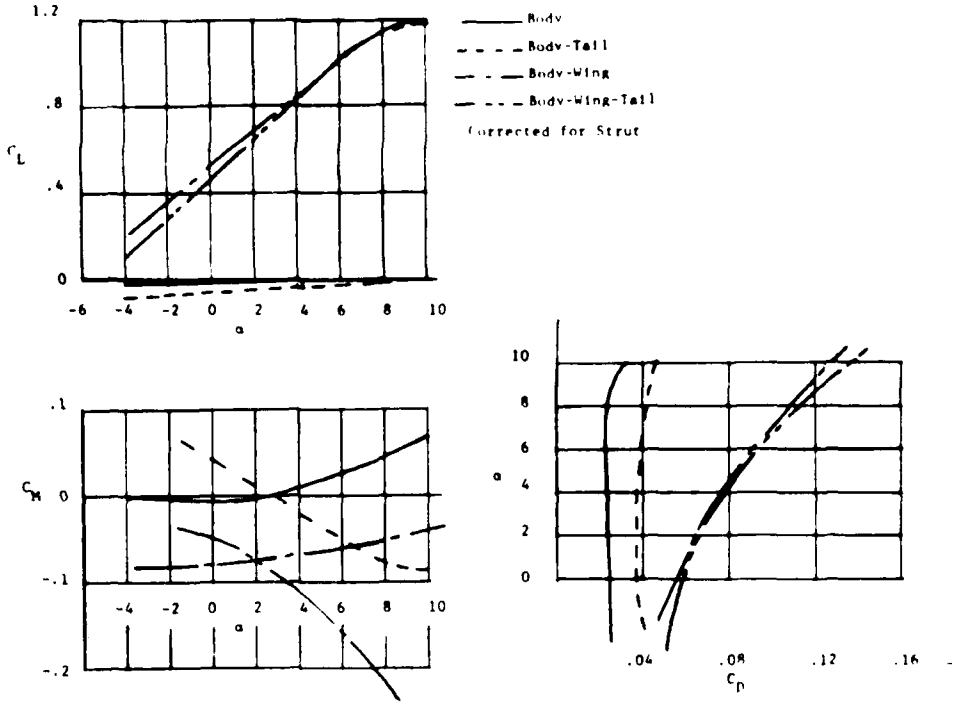

Figure 3 - Longitudinal Build-Up

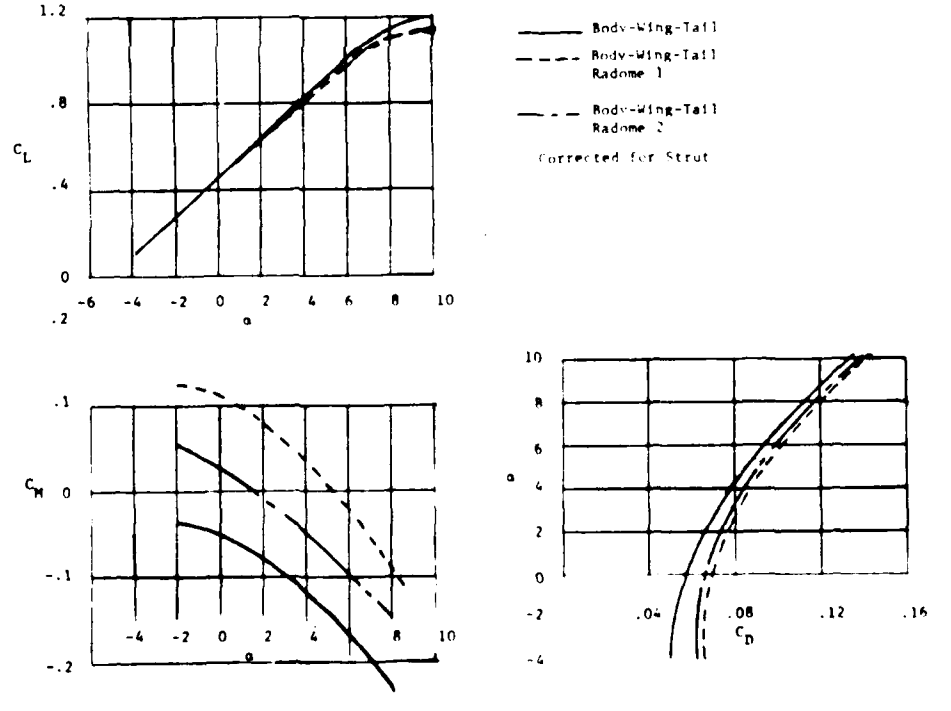

Figure 4 - Effect of Radome

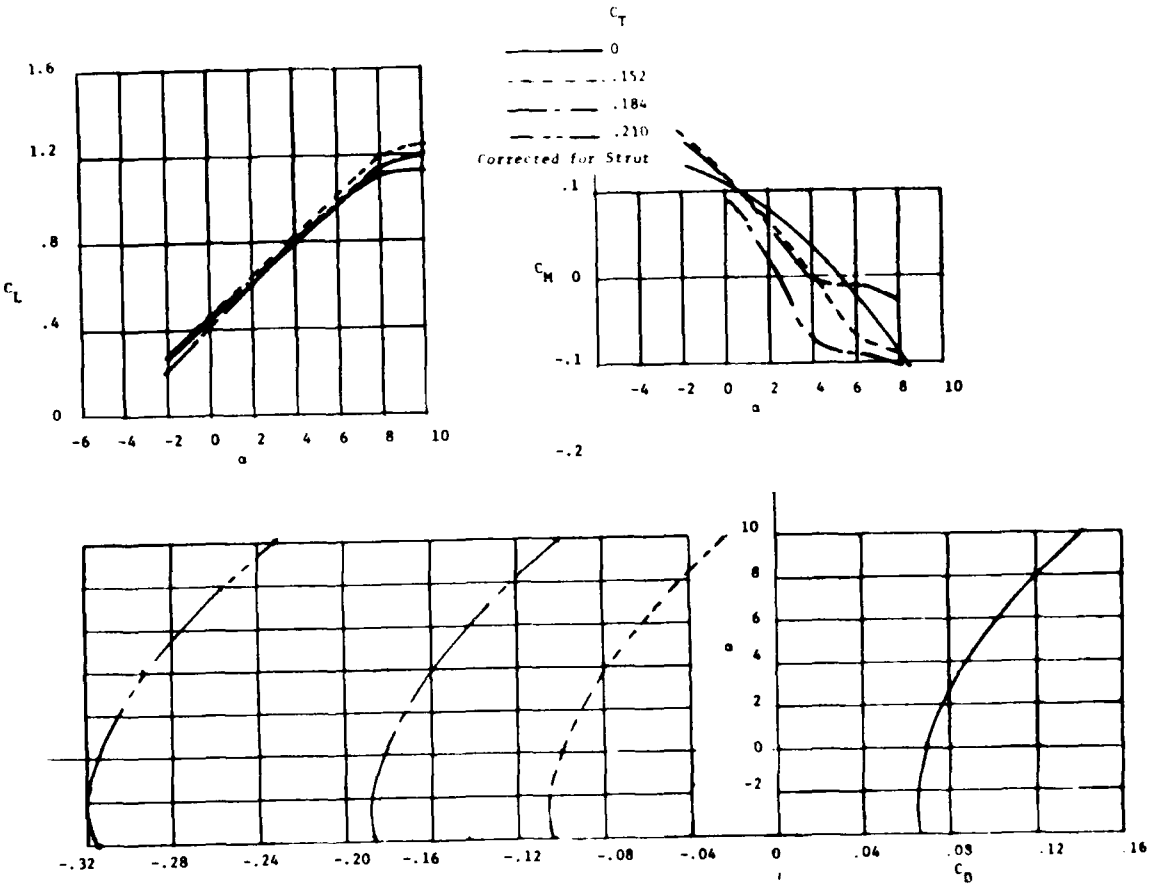

Figure 5 - Effect of Power on Body-Wing-Tail-Radome 1

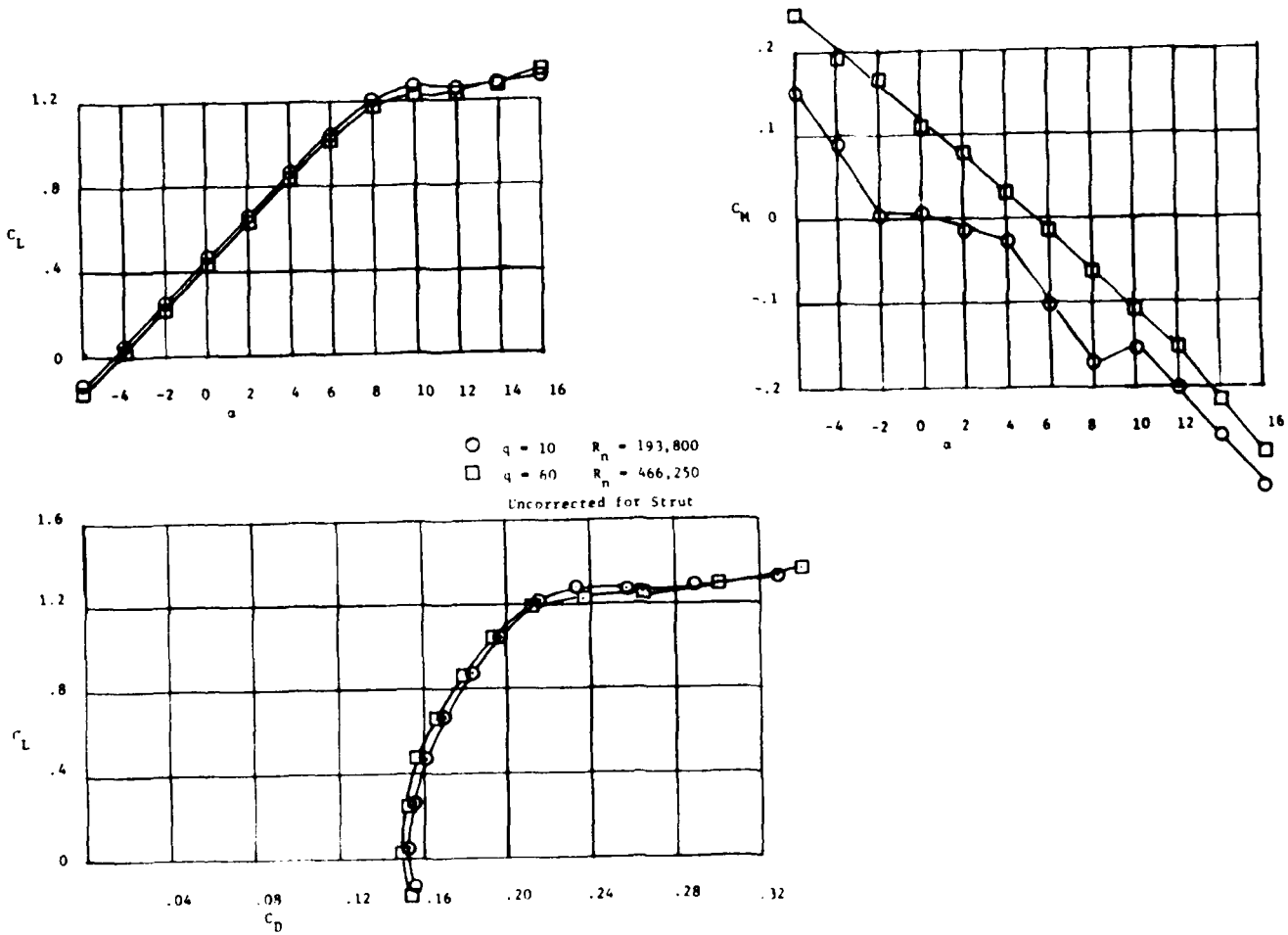

Figure 6 - Effect of Reynolds Number

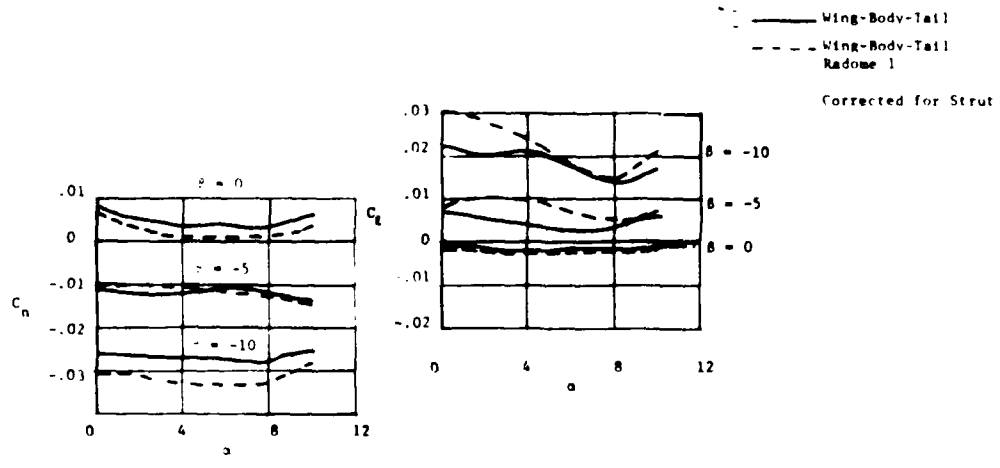

Figure 7 - Lateral Directional Characteristics

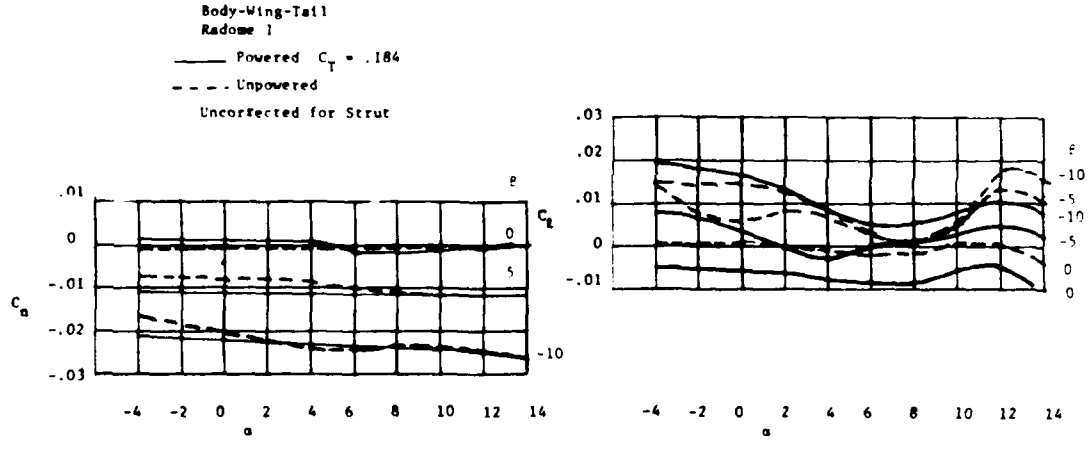

Figure 8 - Effect of Power on Lateral-Directional Characteristics

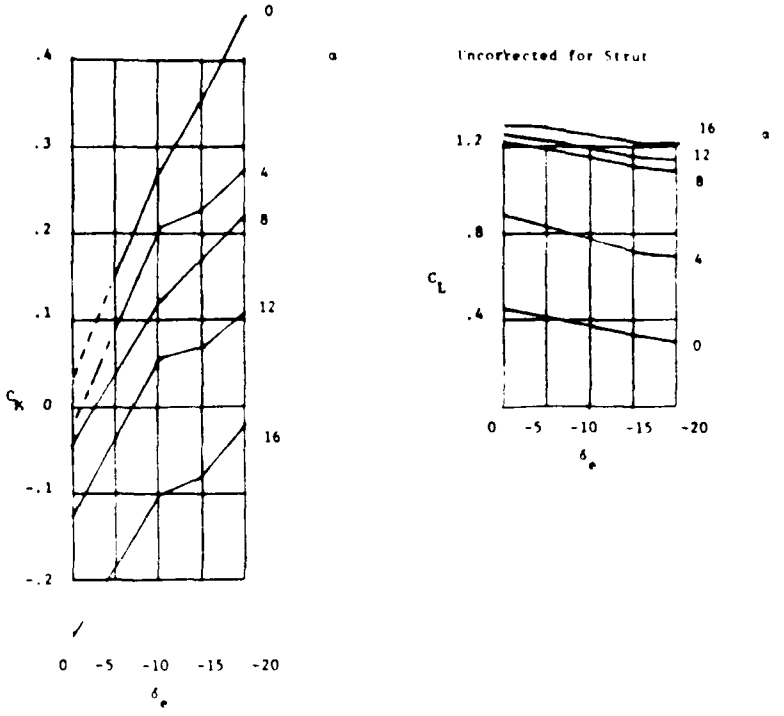

Figure 9 - Elevator Control Power for Wing-Body-Tail-Radome 1

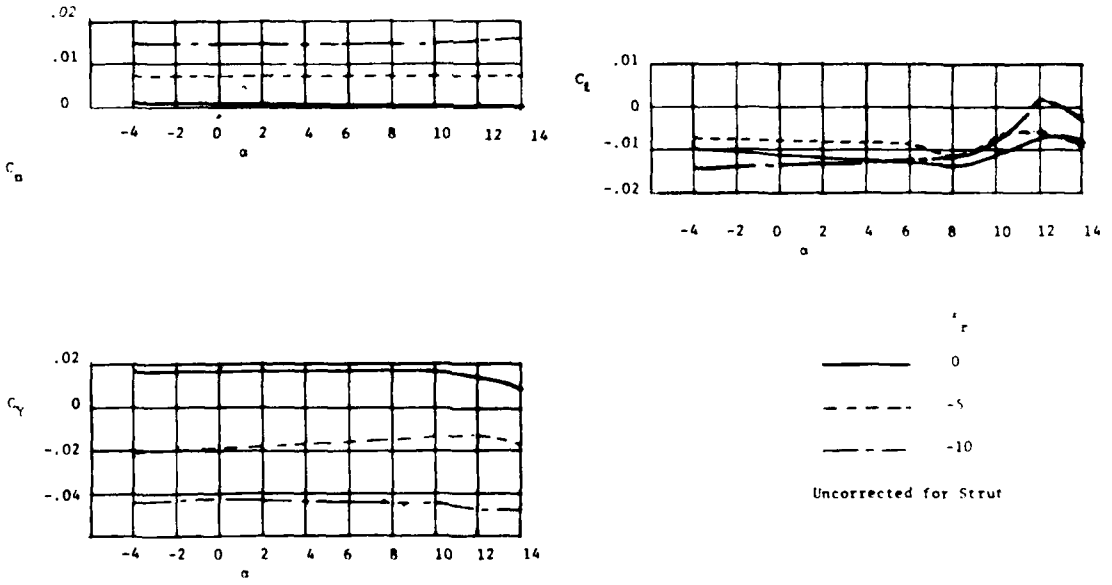

Figure 10 - Powered Rudder Control Effectiveness for Configuration Wing-Body-Tail-Radome 1

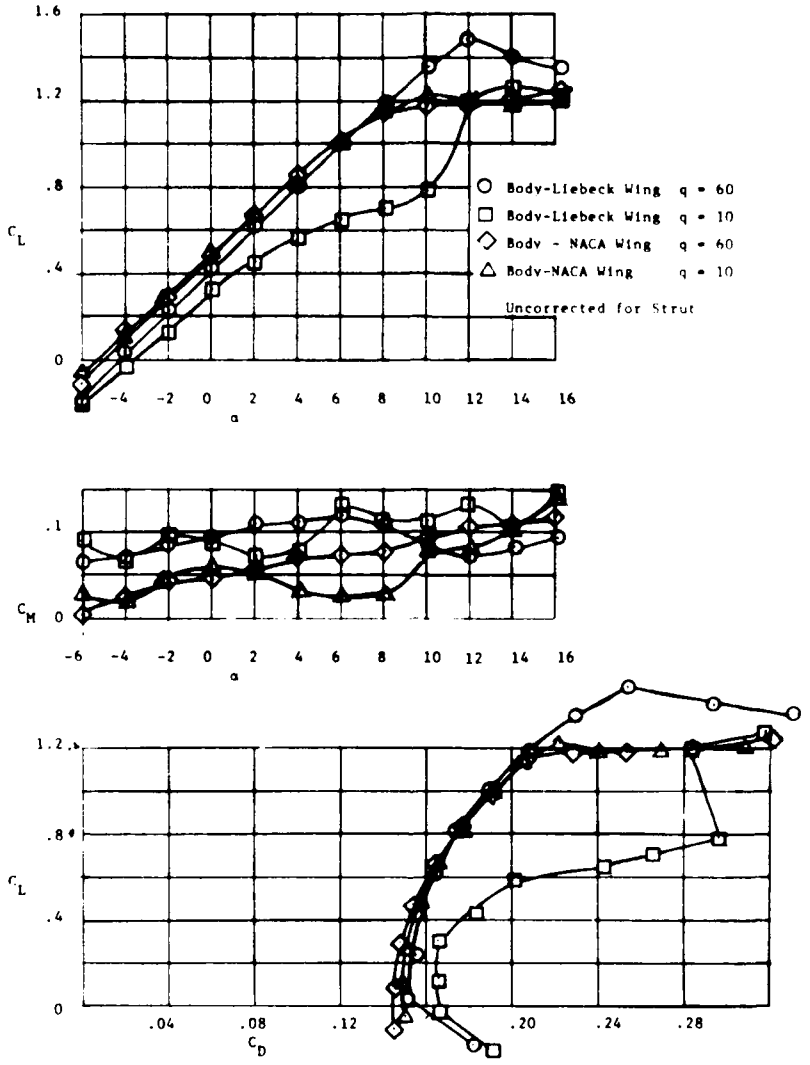

Figure 11 - Comparison of Liebeck and NACA Wings

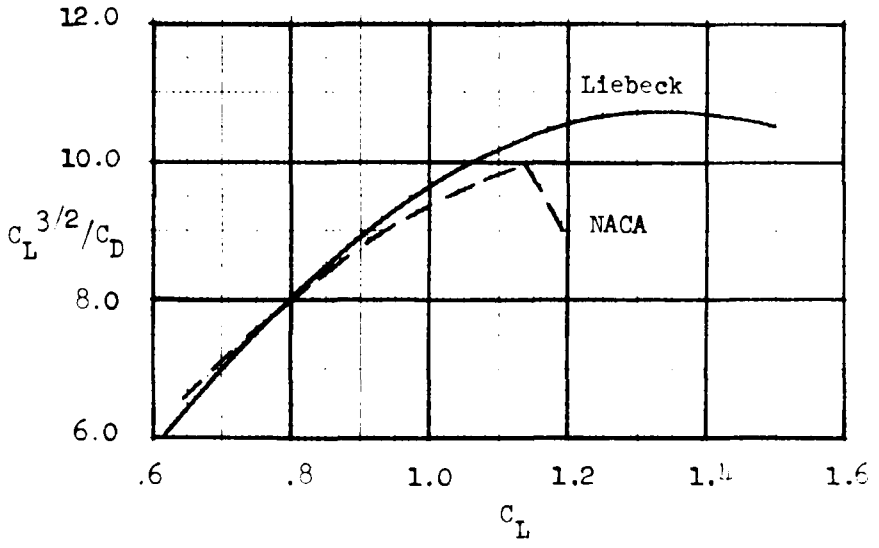

Figure 12 - Comparison of $C_L^{3/2}/C_D$ for NACA and Liebeck Wing Sections

APPENDIX A

SCAT WIND TUNNEL RUN LOG

The following configuration nomenclature was used in the run log to describe the type of model mounting and model configuration:

B	Model with body (fuselage) alone.
BVH	Model with body, vertical and horizontal tails.
WB	Model with body and wing only.
WBVH	Model with body, wing, vertical and horizontal tails.
$WBVHR_1$	Wing, body, vertical and horizontal tails and saucer-shaped radome.
$WBVHR_2$	Wing, body, vertical and horizontal tails and egg-shaped radome.
E	Model in the erect position.
I	Model in the inverted position.
EI	Model erect with image support system installed.

DATA CALCULATION
NDW-NSRDC-3960/9 (156)

DATE

SUBJECT SCAT Wind on Runs

q = 10

A,q = 20 B,q = 30 C,q = 60

SHEET

LINE	COL. A Run No.	COL. B Config No.	COL. C Config	COL. D β°	COL. E Tare No.	COL. F Run No.	COL. J Config No.	Config		Tare
C	003	01 I	WBVH	0	01	059	10 EI	WBVH	0	23
	004	01 I	WBVH	0	01	060	10 EI	WBVH	0	23
A	005	01 I	WBVH	0	01	061	10 EI	WBVH	0	23
B	006	02 I	WBVH	0	01	065	1 I	WBVH	0	24*
	010	03 E	WBVH	0	02	066	1 I	WBVH	5	25*
C	011	03 E	WBVH	0	02	067	1 I	WBVH	10	26
	012	03 E	WBVH	5	03	069	1 I	WBVH	α = 6	27
	013	03 E	WBVH	10	04	073	11 I	WB	0	28
	018	04 E	BVH	0	05	074	11 I	WB	5	29
	019	04 E	BVH	5	06	075	11 I	WB	10	30
	020	04 E	BVH	10	07	079	12 I	B	0	31
	024	05 E	B	0	08	080	12 I	B	5	32
	025	05 E	B	5	09	081	12 I	B	10	33
	026	05 E	B	10	10	085	13 I	BVH	0	34
	030	06 E	WB	0	11	086	13 I	BVH	5	35
	031	06 E	WB	5	12	087	13 I	BVH	10	36
	032	06 E	WB	10	13	091	14 I	$WBVHR_1$	0	37
	036	07 EI	WB	0	14	092	14 I	$WBVHR_1$	5	38
	037	07 EI	WB	5	15	093	14 I	$WBVHR_1$	10	39
	038	07 EI	WB	10	16	094	15 I	$WBVHR_2$	0	37
	042	08 EI	B	0	17	095	15 I	$WBVHR_2$	5	38
	043	08 EI	B	5	18	096	15 I	$WBVHR_2$	10	39
	044	08 EI	B	10	19	097	14 I	$WBVHR_1$	0	37
	049	09 EI	BVH	0	20	098	14 I	$WBVHR_1$	0	37
	050	09 EI	BVH	5	21	099	14 I	$WBVHR_1$	0	37
	051	09 EI	BVH	10	22	100	14 I	$WBVHR_1$	0	37
	055	10 EI	BVH	0	23	101	14 I	$WBVHR_1$	0	37
	056	10 EI	BWVH	5	24	102	14 I	$WBVHR_1$	5	38
	057	10 EI	BWVH	10	25	103	14 I	$WBVHR_1$	10	39
C	058	10 EI	BWVH	0	23	104	14 I	$WBVHR_1$	0	37

CHECKED BY

#60 is repeat of #59

CALCULATED BY

W^1 = Liebeck Wing

MODEL BY

DATA CALCULATION
NDW-NSRDC-3960/9 (156)

DATE

SCAT Wind On Runs

Run No.	Config. No.	Config	β°	Tare No.				
105	14 I	WBVHR;	0	37				
106	14 I	WBVHR;	0	37				
107*	14 I	WBVHR;	0	37				
108*	1 I	WBVH	0	01				
109*	1 I	WBVH	0	01				
110	1 I	WBVH	0	01				
112	1 I	WBVH	α = 0	40				
113	1 I	WBVH	α = 6	27				
114	1 I	WBVH	α = 0	40				
115	1 I	WBVH	0	01				
116	1 I	WBVH	0	01				
117	1 I	WBVH	0	01				
118	11 I	WB	0	28				
120	16 I	W'B	0	41				
121	16 I	W'B	0	41				
123	17 I	W'BVH	0	42				
124	17 I	W'BVH	0	42				
125	1 I	WBVH	0	01				
126	1 I	WBVH	0	01				
127	1 I	WBVH	0	01				
128	14 I	WBVHR;	0	37				
129	14 I	WBVHR;	0	37				
130	14 I	WBVHR;	0	37				
131	14 I	WBVHR;	0	37				
132**	14 I	WBVHR;	0	37				

** 132, no water or motor leads

* #107, 108, & 109 not recorded on Beckman

APPENDIX B

TO ASED 371
WIND TUNNEL RESULTS OF A 10-PERCENT SCALE
POWERED SCAT VTOL AIRCRAFT

(available upon written request to Code 166)

APPENDIX B

FINAL TABULATED FORCE AND MOMENT DATA FOR THE SCAT VEHICLE

The following tabulated data presents the results from the wind tunnel program. The top line gives model configuration data, such as elevator and rudder deflection angle. The second line gives the tunnel conditions at the time force data were recorded. These data include tunnel Mach number, pressures, Reynolds number, and density. The angle of attack and sideslip for each data point precede the force and moment coefficients in stability axis. Tunnel dynamic pressure and velocity follow with the same coefficients presented again, but in wind axis.

DTNSRDC ISSUES THREE TYPES OF REPORTS

(1) DTNSRDC REPORTS, A FORMAL SERIES PUBLISHING INFORMATION OF PERMANENT TECHNICAL VALUE, DESIGNATED BY A SERIAL REPORT NUMBER.

(2) DEPARTMENTAL REPORTS, A SEMIFORMAL SERIES, RECORDING INFORMATION OF A PRELIMINARY OR TEMPORARY NATURE, OR OF LIMITED INTEREST OR SIGNIFICANCE, CARRYING A DEPARTMENTAL ALPHANUMERIC IDENTIFICATION.

(3) TECHNICAL MEMORANDA, AN INFORMAL SERIES, USUALLY INTERNAL WORKING PAPERS OR DIRECT REPORTS TO SPONSORS, NUMBERED AS TM SERIES REPORTS; NOT FOR GENERAL DISTRIBUTION.